THE JOURNAL OF BIOLOGICAL CHEMISTRY VOL. 284, NO. 47, pp. 32846–32857, November 20, 2009

A Mycobacterial Cyclic AMP Phosphodiesterase That Moonlights as a Modifier of Cell Wall Permeability*[S]

Received for publication, July 29, 2009, and in revised form, September 11, 2009 Published, JBC Papers in Press, September 29, 2009, DOI 10.1074/jbc.M109.049635

Marjetka Podobnik[‡1,2], **Richa Tyagi**[§1,3], **Nishad Matange**[§4], **Urška Dermol**[‡4], **Arun K. Gupta**[¶], **Rohini Mattoo**[§], **Kothandaraman Seshadri**[¶], **and Sandhya S. Visweswariah**[§5]

From the [‡]*Laboratory for Biosynthesis and Biotransformation, National Institute of Chemistry of Slovenia, Hajdrihova 19,1000 Ljubljana, Slovenia, the* [§]*Department of Molecular Reproduction, Development and Genetics, Indian Institute of Science, Bangalore 560 012, India, and* [¶]*AstraZeneca India Private Limited, Avishkar Kirloskar Business Park, Bellary Road, Hebbal, Bangalore 560 024, India*

Mycobacterium tuberculosis **utilizes many mechanisms to establish itself within the macrophage, and bacterially derived cAMP is important in modulating the host cellular response. Although the genome of *M. tuberculosis* is endowed with a number of mammalian-like adenylyl cyclases, only a single cAMP phosphodiesterase has been identified that can decrease levels of cAMP produced by the bacterium. We present the crystal structure of the full-length and sole cAMP phosphodiesterase, Rv0805, found in *M. tuberculosis*, whose orthologs are present only in the genomes of slow growing and pathogenic mycobacteria. The dimeric core catalytic domain of Rv0805 adopts a metallophosphoesterase-fold, and the C-terminal region builds the active site and contributes to multiple substrate utilization. Localization of Rv0805 to the cell wall is dependent on its C terminus, and expression of either wild type or mutationally inactivated Rv0805 in *M. smegmatis* alters cell permeability to hydrophobic cytotoxic compounds. Rv0805 may therefore play a key role in the pathogenicity of mycobacteria, not only by hydrolyzing bacterial cAMP, but also by moonlighting as a protein that can alter cell wall functioning.**

Mycobacterium tuberculosis is probably one of the most successful human pathogens known so far, being singly responsible for the largest number of deaths worldwide due to an infectious disease. *M. tuberculosis* is phagocytosed by the macrophage and is able to subvert the defenses of the host by a number of mechanisms. These include the presence of a complex cell wall that prevents free passage of potentially toxic material, the ability of the bacteria to withstand the acidic environment of the phagolysosome, and to neutralize reactive oxygen and nitrogen species produced by the activated macrophage (1). An increased understanding of mechanisms utilized by this pathogen to evade the host immune system and continue to reside in the hostile environment of the macrophage, would no doubt provide avenues for the development of drugs to novel targets in the bacterium.

Cross-communication between the pathogen and host could involve the utilization of signaling molecules that are conserved evolutionarily. Cyclic AMP is found in all kingdoms of life, and proteins that synthesize and degrade the cyclic nucleotide have been well characterized. The genome of *M. tuberculosis* H37Rv encodes 16 mammalian-like nucleotide cyclase-like genes (2), and intracellular and extracellular levels of cAMP are very high in both pathogenic and non-pathogenic (*e.g. Mycobacterium smegmatis*) mycobacteria (2, 3). Recent evidence has highlighted the importance of cAMP in modulating the host macrophage response to *M. tuberculosis* infection (4). A single adenylyl cyclase was shown to be responsible for the burst of cAMP that is seen in the macrophage following phagocytosis of *M. tuberculosis*, and this bacterially derived increase in cAMP was essential to attenuate the response of the macrophage to the pathogen.

The regulated degradation of cAMP is as important as its synthesis, and mammalian cyclic nucleotide phosphodiesterases, classified as Class I enzymes, are the targets for a number of drugs (5). Class I-like enzymes could not be detected in mycobacterial genomes. Instead, we identified a Class III phosphodiesterase, the product of the *rv0805* gene (accession NP_215320), that was capable of degrading mycobacterial cAMP (6). Indeed, overexpression of Rv0805 was used to reduce intracellular levels of cAMP in *M. tuberculosis* to show that bacterially derived cAMP was essential to attenuate macrophage killing (4). Rv0805 is a member of the superfamily of metallophosphoesterases (MPEs)[6] that has been well characterized biochemically and structurally (7–9). MPEs contain five blocks of residues (D-$(X)_n$-GD-$(X)_n$-GNH(E/D)-$(X)_n$-H-$(X)_n$-GHXH) (10) with a conserved structural-fold, containing two metal ions in the active site. These enzymes cleave a variety of

* This work was supported in part by grants from the Slovenian Research Agency (to M. P. and U. D.), the Department of Biotechnology, Government of India, and the Department of Science and Technology, Government of India for an Indo-Slovenian joint project.

[S] The on-line version of this article (available at http://www.jbc.org) contains supplemental Table S1 and Figs. S1–S4.

The atomic coordinates and structure factors (codes 3IB7 and 3IB8) have been deposited in the Protein Data Bank, Research Collaboratory for Structural Bioinformatics, Rutgers University, New Brunswick, NJ (http://www.rcsb.org/).

[1] Both authors contributed equally to this work.

[2] To whom correspondence may be addressed. Tel.: 386-1-476-0372; Fax: 386-1-476-0300; E-mail: marjetka.podobnik@ki.si.

[3] Senior Research Fellow supported by the Council of Scientific and Industrial Research, Government of India.

[4] Considered equal second authors.

[5] To whom correspondence may be addressed. Tel.: 91-80-22932542; Fax: 91-80-23600999; E-mail: sandhya@mrdg.iisc.ernet.in.

[6] The abbreviations used are: MPE, metallophosphoesterase; bis-*p*NPP, bis-(*p*-nitrophenyl)phosphate; pNPPP, *p*-nitrophenyl phenylphosphonate; r.m.s., root mean square; PDB, Protein Data Bank; MES, 4-morpholineethanesulfonic acid; bis-Tris, 2-[bis(2-hydroxyethyl)amino]-2-(hydroxymethyl)propane-1,3-diol.

substrates including phosphomonoesters, phosphodiesters, and phosphotriesters (11), and a single enzyme can cleave multiple substrates *in vitro*. In some cases an unequivocal catalytic function *in vivo* for a particular MPE has been demonstrated. However, Vps29, a protein found in the retromer cargo-recognition complex, has a MPE-fold but no catalytic activity, and instead is used as a scaffolding protein (11–13). By and large, however, the roles of a large number of MPEs remain elusive.

Biochemical and mutational analysis followed by structural studies of the catalytic core of Rv0805 identified residues important for MPE activity and also revealed the close structural similarity between Rv0805 and other MPEs including Ser-Thr phosphatases, Mre11 nuclease, and purple acid phosphatases (14). Our more recent studies have shown that distant orthologs of Rv0805 can also be found in mammalian genomes (15). Intriguingly, the *rv0805* gene is found only in pathogenic mycobacteria (15) and an ortholog is absent in *M. smegmatis*, a non-pathogenic soil mycobacterium, which nonetheless, shows modulation in intracellular cAMP levels. We therefore asked if cAMP was the sole substrate for Rv0805 in mycobacterial cells, and wished to explore the possibility that Rv0805 could be a multifunctional protein, necessitating its presence only in pathogenic mycobacteria. We have now determined the structure of the Rv0805 enzyme, including the C-terminal domain and investigated the functional role of conserved residues by using *in vivo* and *in vitro* assays. We demonstrate that Rv0805 can also utilize a number of phosphodiesters as substrates, and identify the crucial role of the C terminus in building the active site and aiding in localizing the enzyme to the cell envelope in mycobacteria. The structure of Rv0805 in complex with 5′-AMP and docking of substrates into the active site permitted a mutational approach to distinguish residues that are critical for cyclic nucleotide and linear substrate utilization. Finally, overexpression of wild type and mutant Rv0805 in *M. smegmatis* demonstrated that Rv0805 could have a role to play in altering the properties of the cell wall of mycobacteria, independent of its catalytic ability to hydrolyze cAMP, providing a novel line of investigation into hitherto unexplored mechanisms of cell wall construction in mycobacteria.

EXPERIMENTAL PROCEDURES

Protein Purification and Enzymatic Assays—Constructs to express $Rv0805^{1-318}$ and $Rv0805^{1-278}$ have been described earlier (6, 14). The H98A, H140A, H209A, and Y229A mutations were generated on the pPRO-$Rv0805^{1-318}$ plasmid (16). Sequences of mutagenic oligonucleotides are provided in supplemental Table 1.

Wild type and mutant proteins were prepared following addition of $MnCl_2$ and $FeCl_3$ (10 μM) to the bacterial culture medium (14). Assays with bis-(*p*-nitrophenyl)phosphate (bis-*p*NPP), *p*-nitrophenyl phenylphosphonate (*p*NPPP), and *p*-nitrophenyl phosphorylcholine (Sigma) were performed in a triple buffer system (MES, HEPES, diethanolamine, 50 mM, pH 8.5) containing 5 mM 2-mercaptoethanol and 10 mM NaCl in the presence of the specified substrate (10 mM) and 100 μM $MnCl_2$ as metal cofactor (15). Kinetic parameters indicated in the text were calculated by fitting data using GraphPad Prism version 5.00 (GraphPad Software, San Diego, CA). The heat stability of the proteins was measured by incubating $Rv0805^{1-318}$ and $Rv0805^{1-278}$ in assay buffer at 80 °C for the indicated times. Samples were cooled and activity measured following addition of substrate and incubation at 37 °C for 15 min. For circular dichroism experiments, proteins (30 mg/ml) were diluted in 20 mM Tris, pH 8.0, to a final concentration of 0.2 mg/ml and incubated at 80 °C. Aliquots of 200 μl were removed and CD spectra were collected at 37 °C (Chirascan CD Spectrometer, Applied Photophysics, UK).

Crystallization and Structure Determination—$Rv0805^{1-318}$ was expressed in the presence of $MnSO_4$ and $FeCl_3$ (10 μM) in the culture medium and purified as described earlier (14). Samples used for crystallization contained 15–30 mg/ml of Rv0805 protein in 20 mM Tris-HCl, pH 8.0, 50 mM NaCl, and 5 mM 2-mercaptoethanol. Crystals were prepared at 20 °C by hanging drop vapor diffusion, growing from a reservoir solution of 100 mM bis-Tris, pH 6.5 or 7.0, 0.2–0.4 M ammonium acetate, and 50–60% (v/v) 2-methyl-2,4-pentandiol. The crystallization drop size was 2 μl with equal volumes of protein:reservoir solution.

$Rv0805^{1-318}$ was co-crystallized with 5′-AMP by adding 5′-AMP (5 mM) to the reservoir solution. X-ray diffraction experiments were undertaken at EMBL/DESY, Hamburg, beamline BW7A, at 100 K, and wavelengths 1.008 or 0.986 Å, for apo-$Rv0805^{1-318}$ and 5′-AMP-$Rv0805^{1-318}$, respectively. Diffraction data were integrated, scaled, and merged using the HKL2000 package (17) (Table 1). The structure of full-length $Rv0805^{1-318}$ was solved by a combination of molecular replacement (PHASER) (18) with the structure of the catalytic core of $Rv0805^{1-278}$ (Protein data bank 2HY1) as a model (resolution range 32.4-2.5 Å; one clear solution with rotation function *Z*-score 20.9, translation function *Z*-score 64.2, and the log (likelihood) gain 2272), and ArpWarp (18) to build the new structural elements in $Rv0805^{1-318}$. In the case of a complex of $Rv0805^{1-318}$ with 5′-AMP, the structure of the ligand-free $Rv0805^{1-318}$ was used as a model by PHASER (resolution range 31.8-2.5 Å; one clear solution with rotation function *Z*-score 31.4, translation function *Z*-score 61.4, and the log(likelihood) gain 4468). Refinement was undertaken using the REFMAC suite (18) (Table 1) and manual rebuilding of the model in O (19) iteratively. Water molecules were found using ArpWarp and their positions assessed. PyMol (20) was used to prepare the figures. Over 90% of residues were within the allowed regions of the Ramachandran plot. In both structures residues Asp-125 and His-207 are in the disallowed regions, as seen in the structure of the catalytic core $Rv0805^{1-278}$ (14). Moreover, several mostly polar side chains, distant from the active site, have alternative conformations. Values for occupancies for these residues were estimated by varying them during the refinement. In the deposited PDB files, only the conformation with a higher occupancy for each of these residues is included. Occupancy of acetate ion or 5′-AMP bound to the active site metal ions was estimated to be 0.8.

Docking of Substrates—The two-dimensional sketches of bis-*p*NPP, 3′,5′-cAMP, and 2′,3′-cAMP were created using ISIS draw (MDL Information Systems, Inc.), and imported into VIDA (OpenEye Scientific Software) to create SMILES records (21), which were the starting inputs for the LigPrep workflow.

The three-dimensional coordinates of 10 conformers for each ligand were generated and the structure of the $Rv0805^{1-318}$ dimer was subjected to the "protein preparation" wizard of the Schrödinger Maestro (version 8.5, Schrödinger, LLC) with default values. All crystallographically observed solvent molecules were removed keeping only Mn^{2+} and Fe^{3+}. The Receptor-Grid generation module of Glide was invoked to create the docking grid corresponding to the vicinity of 5′-AMP coordinates, incorporating residue information from both Rv0805 protomers. Flexible docking within the grid of all the conformers of the ligands was carried out using the SP option of Glide module. During energy minimization, the ligand atoms were allowed to move, whereas the protein atoms were constrained to their prepared geometry. At least 10 energy optimized poses along with their Glide score were written for each of the ligands.

Expression of $Rv0805^{1-318}$ and $Rv0805^{1-278}$ in M. smegmatis—The $Rv0805^{1-318}$ and $Rv0805^{1-278}$ coding sequences were amplified as described earlier (6), and cloned into pMV10–25 (22), to allow expression of Rv0805 under the mycobacterial *hsp60* gene promoter. A control vector (pMV vector control) was generated by digesting pMV10–25 with NheI and XbaI and religating the vector backbone. Plasmids expressing mutant $Rv0805^{1-318}$ proteins were generated by digesting the respective pPRO-$Rv0805^{1-318}$ plasmids with NcoI and XbaI, isolating the ~900-bp fragment containing the mutation, and replacing the fragment released from similarly digested pMV-Rv0805 1–318 with the fragment containing the mutation. Plasmids were electroporated in *M. smegmatis* and cultured as described earlier (23). Mid-log phase cells of *M. smegmatis* were harvested by centrifugation, washed with 20 mM Tris-HCl, pH 8.5, containing 0.1% Tween 20, and lysed by sonication in buffer containing 200 mM Tris-HCl, pH 8.2, containing 100 mM NaCl, 5 mM β-mercaptoethanol, 4 mM NaH_2PO_4, 10% glycerol, 2 mM phenylmethylsulfonyl fluoride, and 1 mM benzamidine. Subcellular fractions were prepared as described (24). Cell wall and cell membrane fractions were resuspended in lysis buffer and protein content was measured by a modified Bradford procedure (25).

Levels of intracellular and extracellular cAMP were measured as described earlier (23). Phosphodiesterases assays were performed with different subcellular fractions of *M. smegmatis* (50 μg of total protein in the presence of bis-*p*NPP (2 mM) or 2′,3′-cAMP (5 mM)).

Western Blot Analysis—Subcellular fractions prepared from *M. tuberculosis* H37Rv were obtained from the Colorado State University (26). Protein (50 μg) from various subcellular fractions was subjected to 12% SDS-PAGE and blotted onto a polyvinylidene difluoride membrane (Millipore). Monoclonal antibodies against $Rv0805^{1-318}$ were raised and culture supernatants were used at a dilution of 1:100 for blotting with chemiluminescent detection (ECL Plus, GE Healthcare).

Monitoring Cell Wall Permeability—Approximately 10^7 cells (based on optical density measurements) from mid-log phase cultures of each strain were spotted onto 7H10 agar plates containing 5 μg/ml of malachite green, 10 μg/ml crystal violet (MP Biomedicals), or 0.01% SDS. The plates were incubated at 37 °C for 2–3 days and photographed.

TABLE 1
Data collection and refinement statistics
Each structure was determined using diffraction data by one crystal.

	$Rv0805^{1-318}$	5′-AMP-$Rv0805^{1-318}$
Data collection		
Space group	$P4_12_12$	$P4_12_12$
Cell dimensions		
a, *b*, *c* (Å)	100.18, 100.18, 80.25	100.40, 100.40, 80.80
Resolution (Å)	50-1.60 (1.64-1.60)[a]	50-1.80 (1.84-1.80)
R_{merge}	5.7 (52.8)	6.7 (61.9)
$I/\sigma I$	34.9 (2.3)	29.5 (3.7)
Completeness (%)	99.9 (99.6)	99.9 (100.0)
Redundancy	9.4 (5.0)	8.0 (7.7)
Refinement		
Resolution (Å)	32.4-1.6 (1.64-1.60)[a]	31.8-1.8 (1.85-1.80)
No. reflections ($F > 0\sigma$)	54,293	38,804
R_{work}/R_{free}	15.9/17.7 (31.1/33.1)	15.0/16.8 (20.4/25.7)
No. atoms[b]		
Protein	2,229	2,229
Ligand/ion		
Iron	1	1
Manganese	1	1
Bis-Tris	14	14
5′-AMP (active site)		23
Acetate (active site)	4	
MPD	16 (2 molecules)	24 (3 molecules)
Acetate	4	4
Water	292	247
B-factors		
Protein	24.3	26.5
Ligand/ion		
Iron	14.3	17.0
Manganese	14.4	16.7
Bis-Tris	20.7	23.9
5′-AMP (active site)		29.2
Acetate (active site)	16.1	
MPD	42.1	55.9
Acetate	54.9	64.7
Water	33.9	34.8
Wilson *B*-factor	26.6	29.1
R.m.s. deviations		
Bond lengths (Å)	0.008	0.009
Bond angles (°)	1.16	1.24

[a] Values in parentheses are for highest-resolution shell.
[b] Values for asymmetric unit, containing one monomer of the dimer. The dimer is generated using symmetry operation Y, X, −Z.

RESULTS

Promiscuity of Rv0805 in Substrate Utilization—Earlier preparations of Rv0805 resulted in mixtures of monomeric and dimeric forms, with dimerization dependent on the occupancy of the active site with the metal ions (14). Inclusion of Mn^{2+} and Fe^{3+} in the medium in which expression of recombinant Rv0805 was performed now resulted in >95% of dimeric purified Rv0805, which was enzymatically active without the addition of extra Mn^{2+} during the assay (data not shown). Rv0805

TABLE 2
Promiscuous substrate utilization of $Rv0805^{1-318}$ and $Rv0805^{1-278}$
Assays were performed three times in duplicate and values shown represent the mean ± S.E.

	Bis-*p*NPP		*p*NPPP		3′,5′-cAMP		2′,3′-cAMP	
	K_m	V_{max}	K_m	V_{max}	K_m	V_{max}	K_m	V_{max}
	mM	μmol/min/mg	mM	μmol/min/mg	mM	μmol/min/mg	mM	μmol/min/mg
$Rv0805^{1-318}$	0.9 ± 0.08	74 ± 0.8	0.9 ± 0.1	112.7 ± 5	5.5 ± 1	1.1 ± 0.1	1 ± 0.03	14.7 ± 0.25
$Rv0805^{1-278}$	0.3 ± 0.04	10.2 ± 1	1.06 ± 0.14	27.8 ± 2.75	7.5 ± 1.26	1.1 ± 0.09	2.8 ± 0.36	14.2 ± 0.17

hydrolyzed multiple substrates (Table 2), and could cleave *p*-nitrophenyl phosphorylcholine efficiently (V_{max} 41.7 ± 0.15 μmoles/min/mg of protein; K_m 3.3 ± 0.18 mM), and thymidine 5′-monophosphate-*p*-nitrophenyl ester to low extents (~5–10% of the activity seen with bis-*p*NPP). Cleavage of *p*NPPP (Table 2) with the formation of *p*-nitrophenol (*p*NP) demonstrates that a phosphorus center with only three oxygen atoms suffices for phosphoester hydrolysis. 2′,3′-cAMP was a better cyclic nucleotide substrate than 3′,5′-cAMP, with the products of hydrolysis of 3′,5′-cAMP being 5′- and 3′-AMP in a ratio of 2:1, whereas 2′,3′-cAMP was hydrolyzed to 3′- and 2′-AMP in a ratio of 4:1 (supplemental Fig. S1). A recent report has shown that 2′,3′-cGMP is also hydrolyzed by Rv0805 as efficiently as 2′,3′-cAMP (9), indicating that there may be no specific interaction of the protein with the base of the cyclic nucleotide. To appreciate the features in Rv0805 that allow this wide substrate utilization, we decided to understand the structural properties of the full-length enzyme and identify residues that are important for substrate binding.

Structure of Rv0805$^{1-318}$—Newly purified full-length Rv0805 protein (residues 1–318; Rv0805$^{1-318}$) readily and rapidly formed proteolytically stable crystals. Mass spectrometric analysis and N-terminal amino acid sequencing of the new crystals demonstrated that the protein was of the size predicted for the Rv0805$^{1-318}$ construct (supplemental Fig. S2). The protein that was crystallized earlier as the Rv0805 catalytic core (14) contained residues 1–278, which we refer to here as Rv0805$^{1-278}$. The structure of Rv0805$^{1-278}$ was defined only for residues Pro^{10}–Pro^{265}, excluding loops Gly^{26}–Val^{35} and Tyr^{229}–Gln^{247} (supplemental Fig. S2).

Rv0805$^{1-318}$ forms a homodimer, with the protomers related by a 2-fold crystallographic axis (Fig. 1*A*). Electron density was well defined for residues Leu^{4}–Asp^{298}, which now reveal several new structural features not previously seen in the structure of the catalytic core. These include a short stretch of residues (Leu^{4}–His^{9}) at the N terminus as well as loops Gly^{26}–Val^{35} and Tyr^{229}–Gln^{247} (Fig. 1, *A*–*C*). The solvent-exposed stretch of residues Leu^{4}–Asp^{13} runs almost parallel and in the same direction as the C-terminal residues of the same protomer (Gly^{289}–Asp^{298}) with several hydrogen bonds between the residues of these two regions (Fig. 1*D*). The N terminus is also held in place by polar interactions to the residues of the other protomer (Fig. 1*D*). Two additional loops that are now defined in Rv0805$^{1-318}$ are stabilized by the presence of C-terminal residues Leu^{266}–Asp^{298} of the other protomer (Fig. 1, *A* and *E*). The lack of ordered structure for residues beyond Asp^{298} in Rv0805$^{1-318}$ is either due to the absence of stabilization of these residues by other parts of the dimer (Fig. 1, *A* and *D*) or the absence of contacts with symmetry related molecules in the crystal.

Intra- and inter-protomer interactions lead to swapping of structural elements between the two protomers (Fig. 1, *A* and *D*). The lasso-shaped loop Tyr^{229}–Gln^{247} is sandwiched between the Gly^{26}–Val^{35} loop and the hydrophobic region Val^{176}–Val^{181} including helix α5 of the same protomer. Furthermore, it leans on the C-terminal part of the helix α1 and is capped by the residues of the C-terminal peptide (Leu^{266}–Pro^{278}), both belonging to the other protomer (Fig. 1, *A* and *B*). The loops Gly^{26}–Val^{35} and Tyr^{229}–Gln^{247} from one protomer form a channel, filled by the capping stretch of the C-terminal domain of the other protomer (Fig. 1*E*). These three structural elements in Rv0805$^{1-318}$ are interconnected via hydrogen bonds as well as hydrophobic interactions, and build a wall beyond the active site (Fig. 1, *A*, *B*, and *E*).

The C-terminal peptide is mainly built of a coil, with residues Pro^{278}–Ser^{288} forming the only α helix in this domain, α7 (Fig. 1). α7 helix stacks against the hydrophobic α5 helix of the other protomer in a parallel manner, pointing in the same direction. The amino acid sequence of the C-terminal domain of Rv0805 is unique to this protein and therefore results in a fold that is distinct from that seen in other MPEs such as Mre11 (7) or GpdQ (11).

The core MPE domain of Rv0805$^{1-318}$ superimposes closely to Rv0805$^{1-278}$ (r.m.s. deviation value for Cα atoms of residues Arg^{40}–Pro^{220} is 0.48 Å), but with significant shifts in particular parts of the structure. In Rv0805$^{1-318}$, a hydrophobic stretch of residues at the N-terminal part of the α5 helix (Ile^{173}–Val^{183}) is pressed down toward the active site by the α7 helix of the other protomer (supplemental Fig. S3). This new feature helps to engage Tyr^{210} of the same protomer in one fully occupied conformation via a hydrogen bond between the OH group of Tyr^{210} and OG atom of Ser^{175} and amide N of Val^{176}. In the Rv0805$^{1-278}$ structure, the absence of interaction with Tyr^{210} caused it to flip between two equally occupied conformations (14). Flipping is additionally prevented in Rv0805$^{1-318}$ by the presence of the Tyr^{229}–Gln^{247} loop of the same protomer placed above Tyr^{210} (supplemental Fig. S3).

Another significant difference is located in loop Val^{136}–Gly^{142}, at the His^{139} and His^{140} positions (supplemental Fig. S3). Although one of the reasons for this difference may be the presence of the new structural elements in Rv0805$^{1-318}$, this could also be caused by the molecule of bis-Tris from the crystallization solution, which binds close to these residues in Rv0805$^{1-318}$ (supplemental Fig. S3).

Swapped Structural Elements in Rv0805—Domain swapping in proteins occurs at positions where the protein tends to locally unfold prior to complete unfolding (27). The two structural elements that are directly involved in domain swapping in Rv0805$^{1-318}$ are loop Tyr^{229}–Gln^{247} of one protomer and Leu^{266}–Ile^{290} in the C-terminal peptide of the other protomer, including the α7 helix (Fig. 1). The N-terminal part of the α7 helix at Pro^{278} is positioned above the tip (residues ^{236}AAGG^{239}) of loop Tyr^{229}–Gln^{247} of the other protomer.

To test if additional structural elements in Rv0805$^{1-318}$ affect the stability of the protein in comparison to the catalytic core, we monitored the activity of both Rv0805 constructs following incubation at 80 °C. The activity of Rv0805$^{1-318}$ was dramatically reduced following 5 min of incubation and completely lost after 30 min (Fig. 2*A*). On the other hand, elevated temperatures did not significantly affect the activity of Rv0805$^{1-278}$. Circular dichroism showed severe changes in the secondary structure of Rv0805$^{1-318}$ after short incubation times, whereas the spectra of Rv0805$^{1-278}$ showed structural changes only after 2 h of incubation at 80 °C (Fig. 2*B*). Therefore, it is likely that the C terminus might play the role of a local unfolding center because the absence of this sequence in Rv0805$^{1-278}$ renders the protein significantly more stable than the full-length

enzyme. This feature may also account for the proteolytic cleavage of Rv0805$^{1-318}$ at Pro^{278} into Rv0805$^{1-278}$ seen in our earlier preparations of recombinant protein (14).

Active Site of Rv0805$^{1-318}$ and a Complex with 5′-AMP—The structure of Rv0805$^{1-318}$ reveals new structural elements that significantly contribute to the architecture of the active site.

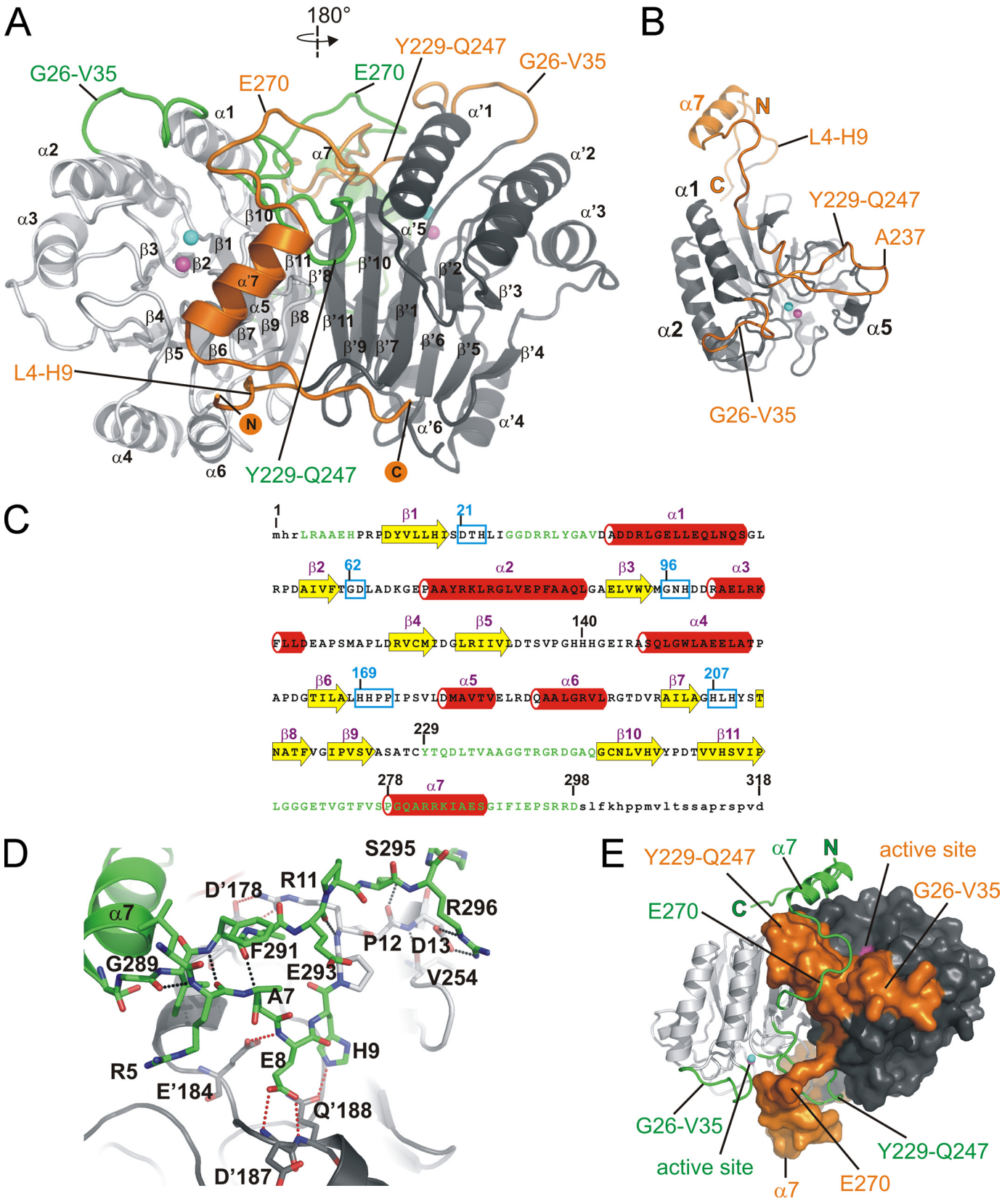

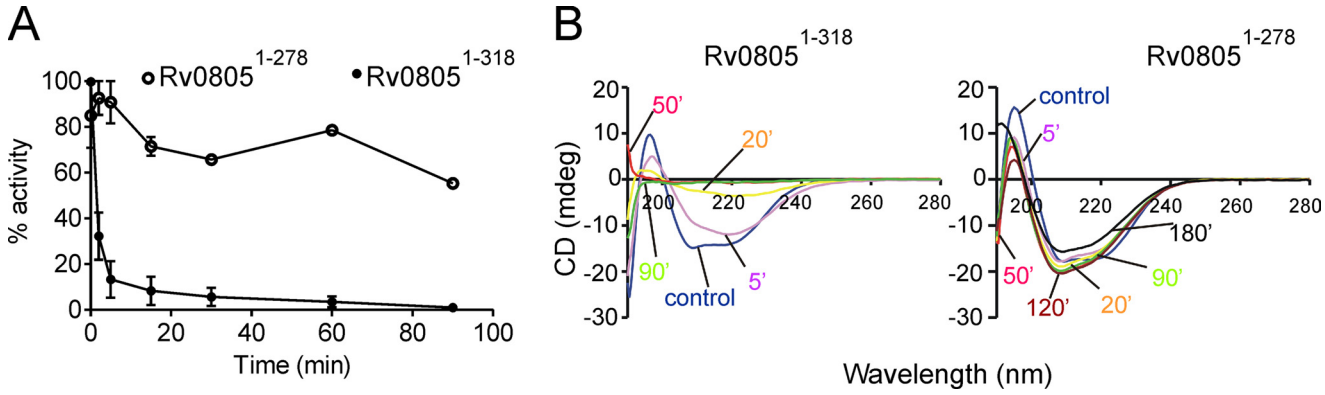

FIGURE 2. **Thermal stability of Rv0805.** *A*, purified Rv0805$^{1-318}$ and Rv0805$^{1-278}$ proteins (1 μg each) were incubated at 80 °C in assay buffer, in the absence of substrate. At the indicated times, an aliquot was removed and chilled on ice. Assays were performed on all samples at the end of incubation by addition of bis-*p*NPP as the substrate. *B*, circular dichroism spectra were collected at 37 °C after incubation of proteins at 80 °C at the indicated times. *Control*, spectrum at 37 °C with no preincubation at 80 °C.

Whereas the active site appeared broad and open to the solvent in Rv0805$^{1-278}$, loops Gly^{26}–Val^{35} and Tyr^{229}–Gln^{247} in the Rv0805$^{1-318}$ frame the active site by forming a rim (Fig. 3*A*). Residues Tyr^{32}, Tyr^{229}, and Gln^{231} constitute a network of hydrogen bonds between each other and the active site metals, either directly or through water molecules, thereby keeping the active site in place (Fig. 3*C*). However, the main structural organizer of the architecture of the Rv0805$^{1-318}$ active site rim is the C-terminal domain (Leu^{266}–Asp^{298}) of the other protomer which, as the main domain-swapped structural element, folds on top of the active site (Figs. 1*A* and 3). The active site of Rv0805$^{1-318}$ contains an acetate ion bound to the metal ions in the similar bidentate manner (Fig. 3*C* and supplemental Fig. S3) as the phosphate ion seen earlier in Rv0805$^{1-278}$ (14), resulting from a relatively high concentration of acetate in the crystallization solution (0.2–0.4 M).

To appreciate the role of this C-terminal domain in regulating the activity of Rv0805, we purified Rv0805$^{1-278}$ in a manner similar to Rv0805$^{1-318}$, and monitored the activity of both proteins to a variety of substrates (Table 2). Rv0805$^{1-278}$ showed similar activity as the full-length enzyme for substrates containing the *cyclic* phosphodiester bond, such as 2′,3′-cAMP and 3′,5′-cAMP. However, Rv0805$^{1-278}$ had a lower activity than Rv0805$^{1-318}$ with the larger colorimetric substrates containing a *linear* phosphodiester bond, emphasizing the important structural contribution made by the C terminus of Rv0805 to the active site.

We were able to co-crystallize Rv0805 in the presence of 5′-AMP, thus providing a visualization of product in the active site of a cyclic nucleotide MPE. 5′-AMP is buried deeply in the active site pocket, with the purine base in a *syn*-conformation and the ribose ring in the C_3-endo-conformation (Fig. 3, *B* and *D*, and supplemental Fig. S4). Its main anchor to the active site is through its phosphate group that is bound to the active site in a similar manner to that of free phosphate in Rv0805$^{1-278}$ (14). The phosphate moiety of 5′-AMP makes contacts to several water molecules in the active site, including the planar active site water, to both metals ions, and directly to side chains of His^{23}, Asp^{63}, Asn^{97}, and His^{98} (Fig. 3*D*). There is no direct interaction with any of the side chains of Rv0805 with the purine base or with the ribose ring, in agreement with the earlier observation that cGMP was utilized as efficiently as a substrate by Rv0805 (6, 9). The purine ring is placed parallel to the short hydrophobic helix α5 of the protomer in which the active site is located. The ribose and the purine rings are, however, involved in indirect hydrogen bonding via water molecules to both protomers (Fig. 3*D*). It is likely that the sum of all these interactions is substantial and thus responsible for the poor release of 5′-AMP from the active site and therefore relatively low rate of hydrolysis of 3′,5′-cAMP (Table 2 and supplemental Fig. S1*B*). Binding of 5′-AMP does not result in any major changes of the active site architecture. The mode of binding of 5′-AMP is very similar to binding of dAMP, a product of an exonucleolitically cleaved DNA end in Mre11 (7), which supports a common phosphoesterase mechanism between members of the MPE family.

We attempted to prepare crystals of Rv0805 in the presence of either 2′,3′-cAMP or 3′,5′-cAMP. Binding of these ligands in any of these crystal forms was not well defined, but due to the tetrahedral shape of the electron density above the metal ions in these structures, we assume that the cyclic nucleotides were hydrolyzed to their corresponding monophosphates during complex formation in crystals. However, the shape of the electron density in the place of a ribose and purine did not allow

FIGURE 1. **Crystal structure of the Rv0805$^{1-318}$ homodimer.** *A*, ribbon representation of the Rv0805$^{1-318}$ dimer. The MPE catalytic core is colored *light gray* (left-side protomer) or *dark gray* (right-side protomer). New structural elements are colored *orange* (*attached to the dark gray catalytic core*) or *green* (*attached to the light gray catalytic core*). N and C termini of the *dark gray*/*orange* protomer are marked. α-Helices and β-sheets are indicated, *dark gray*/*orange* protomer with a *prime*. Active site metals ions are shown as *spheres*: Fe^{3+}, *cyan*; Mn^{2+}, *magenta*. *B*, Rv0805$^{1-318}$ monomer: catalytic core, *dark gray*; new structural elements, *orange*. Active site metals are shown as in *A*. *C*, secondary structure elements of Rv0805$^{1-318}$ monomer superimposed onto the amino acid sequence (β-strands, *yellow arrows*; α-helices, *red cylinders*). Newly defined parts of the Rv0805$^{1-318}$ structure are in *green*. Highly conserved MPE family regions are highlighted by *cyan boxes* and several residues indicated in the text are *numbered*. *Small letters* represent parts of the structure that are not defined by electron density. *D*, polar interactions: between N-terminal and C-terminal residues of the same protomer (*black dashed lines*); between N-terminal peptide of one protomer and residues of the other protomer (*red dashed line*). Residues of the protomer in *dark gray*/*orange* combination are marked with a *prime* (*i.e. D′187*) and the *light gray*/*green* protomer as normal (*i.e. D13*). *E*, swapped structural elements between the protomers in the Rv0805$^{1-318}$ dimer. Color code is the same as in *A*. Protomer colored *dark gray*/*orange* is shown as a surface and the *light gray*/*green* protomer as ribbon.

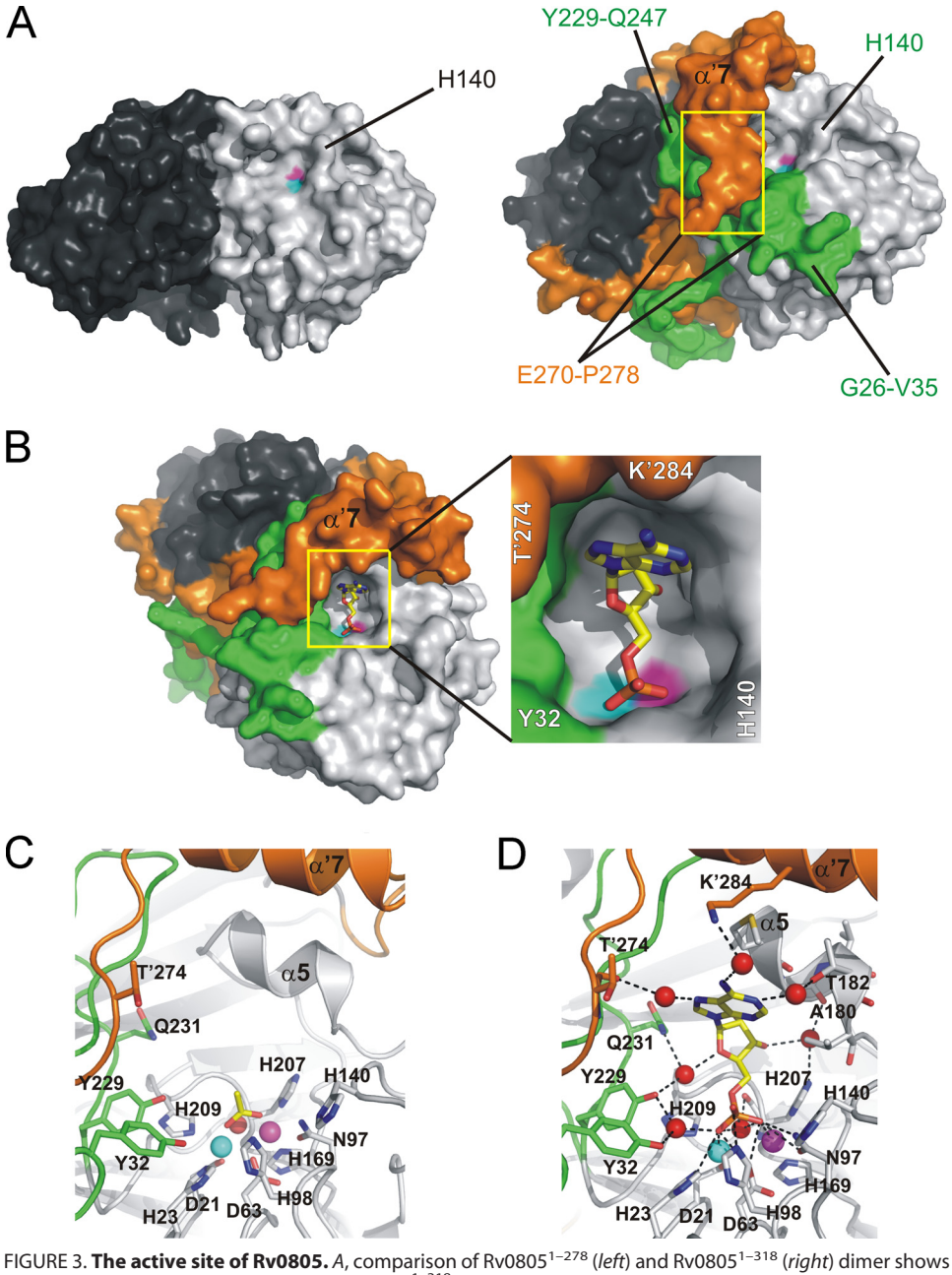

FIGURE 3. **The active site of Rv0805.** *A*, comparison of Rv0805$^{1-278}$ (*left*) and Rv0805$^{1-318}$ (*right*) dimer shows a significant closure of the active site in Rv0805$^{1-318}$. In this view, only one of the two equal active sites is seen (*light gray/green* protomer). *Yellow rectangles* cover the regions of residues Glu′^{270}-Pro′^{278} that run into α′7 helix from the *bottom up*. *B*, Rv0805$^{1-318}$ active site with bound 5′-AMP (*left panel*). 5′-AMP is shown as *sticks* (carbon, *yellow*; oxygen, *red*; nitrogen, *blue*; phosphorus, *orange*). *Middle panel*, zoom of the active site. *C*, zoom of the active site showing acetate in sticks bound to Rv0805$^{1-318}$ (carbon, *yellow*; oxygen, *red*; *spheres* are Fe^{3+}, *cyan*; Mn^{2+}, *magenta*; planar active site water, *red*). *D*, 5′-AMP-Rv0805$^{1-318}$ complex. For the 5′-AMP complex, polar interactions with the active site residues, metals, and water molecules are shown. Color code is the same as described in the legend to Fig. 1, residues of the protomer in *dark gray/orange* combination are marked with a *prime*.

unambiguous modeling of the nucleotides. Preparation of crystals in the presence of 2′-AMP or 3′-AMP did not result in complex formation.

Docking of Substrates in the Active Site of Rv0805$^{1-318}$ and Mutational Analysis—Molecular docking results with multiple substrates in the new high resolution structure of the active site of Rv0805 (Fig. 4) differ significantly to studies reported earlier (9, 14), largely because the previous docking was performed on the crystal structure of Rv0805$^{1-278}$, which was incomplete in detail in the absence of the C terminus. The phosphate oxygen atoms of all substrates are at coordinating distances (2.1–3.3 Å) from both Fe^{3+} and Mn^{2+}, indicating the critical positioning of the phosphorous atom in the binding site. Asn^{97} side chain hydrogen bonds to the phosphate moiety of all substrates, the exception being the interaction with 3′,5′-cAMP in an orientation that yields 5′-AMP as a product (Fig. 4*B*). Here, Asn^{97} is in hydrogen bonding distance with the ribose hydroxyl group (O2). Asn^{97} also stabilizes the phosphate moiety of the product 5′-AMP (Fig. 3*D*). In agreement with the critical role for this residue, the N97A mutant shows no activity with bis-*p*NPP or 3′,5′-cAMP, and only 2% activity of wild type with 2′,3′-cAMP (Fig. 4*E*).

Docking of 3′,5′-cAMP resulted in two equally possible positions of this substrate (Fig. 4, *A* and *B*), explaining the almost equal ratios of 3′- and 5′-AMP formed on hydrolysis by Rv0805$^{1-318}$ (supplemental Fig. S1*B*). The distance between NE2 of His^{98} and the oxygen from the phosphodiester bond of 3′,5′-cAMP is ~3–3.5 Å (Fig. 4, *A* and *B*), allowing stabilization of the transition state and release of 3′-AMP or 5′-AMP as product. The phosphodiester bond in the lowest energy model of 2′,3′-cAMP (Fig. 4*C*) is oriented toward, but placed farther, from His^{98} than in both potential orientations of 3′,5′-cAMP. The phosphodiester bond in bis-*p*NPP points away from the His^{98} side chain (Fig. 4*D*), suggesting that His^{98} could have an important role in facilitating hydrolysis of 3′,5′-cAMP and 2′3′-cAMP, but not bis-*p*NPP. Indeed, the H98A mutant protein showed significant activity (~60% of wild type activity) with bis-*p*NPP as substrate (Fig. 4*E*). In contrast, a dramatic reduction in activity was seen with both 3′,5′-cAMP and 2′,3′-cAMP. The importance of His^{98} in contributing to 2′,3′-cAMP hydrolytic activity has been alluded to earlier (9).

The purine ring in the docked 3′,5′-cAMP molecule does not make any direct contact with the protein. In contrast, the N6 of the purine ring of 2′,3′-cAMP is predicted to form hydrogen bonds to the carbonyl oxygen of Thr^{274} of the other protomer,

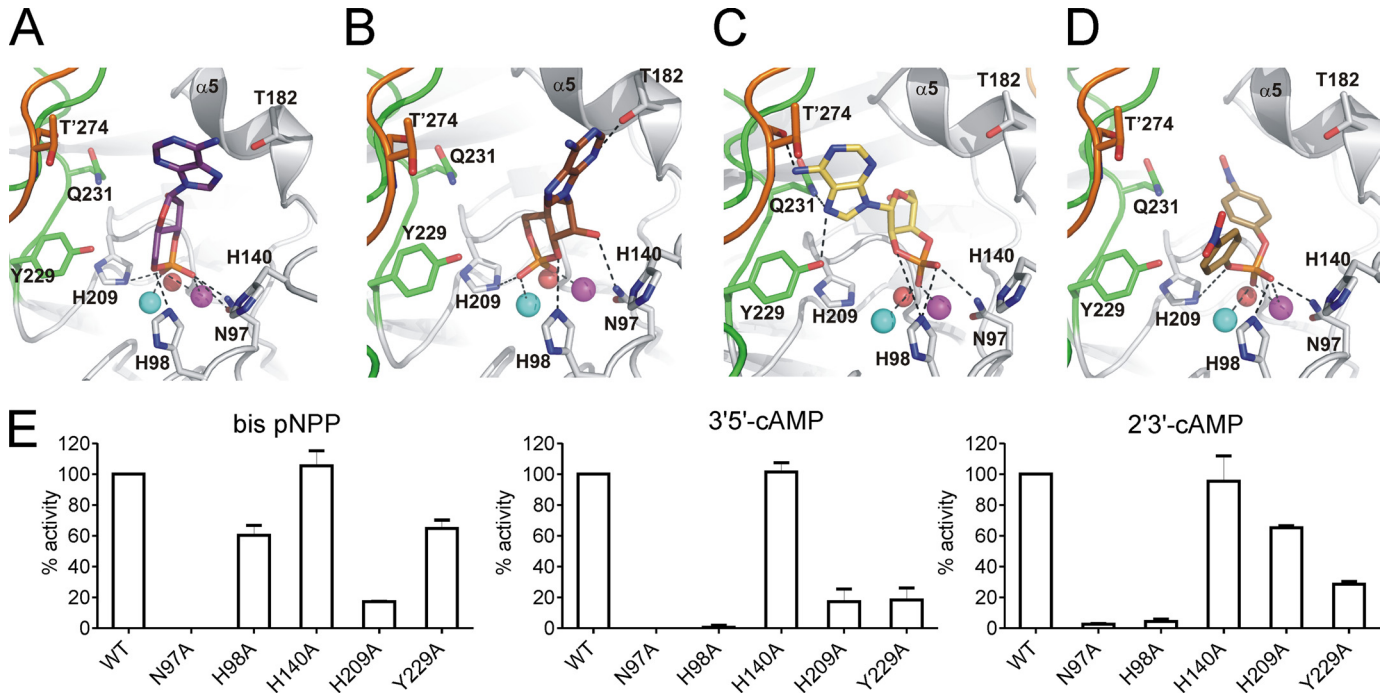

FIGURE 4. **Docking of substrates into the active site of Rv0805$^{1-318}$ dimer.** *A*, 3′,5′-cAMP in orientation that releases 3′-AMP upon hydrolysis. *B*, 3′,5′-cAMP in orientation that releases 5′-AMP upon hydrolysis. *C*, 2′,3′-cAMP in orientation that releases 3′-AMP upon hydrolysis. *D*, bis-*p*NPP in an orientation that releases pNP upon hydrolysis. In all panels, potential polar interactions are depicted as *dashed black lines*. Color code for the protein is the same as in Fig. 1. Substrates are shown as *sticks*. Oxygen, *red*; nitrogen, *blue*; phosphorus, *orange*; carbon, *violet*, 3′,5′-cAMP in *A*; *brown*, 3′,5′-cAMP in *B*; *yellow*, 2′,3′-cAMP in *C*; *dark yellow*, bis-*p*NPP in *D*. Fe^{3+} (*cyan*), Mn^{2+} (*magenta*), and planar active site water (*red*) are shown as *spheres*. Residues of the protomer in *dark gray/orange* combination are marked with a *prime*. *E*, wild type or mutant Rv0805$^{1-318}$ proteins were assayed with the substrates indicated. Values represent the mean ± S.E. of assays repeated three times in duplicate, with two different batches of proteins, and are normalized to the activity seen with the wild type protein.

and the N7 atom is also in hydrogen-bonding distance with a hydroxyl group of Tyr^{229} and side chain amide of Gln^{231} (Fig. 4*C*). These multiple interactions could account for the more optimal use of 2′,3′-cAMP as a substrate for Rv0805. The almost exclusive formation of 3′-AMP as the product of hydrolysis of 2′,3′-cAMP can be explained by the fact that an opposite orientation of 2′,3′-cAMP in the active site (which would yield 2′-AMP as a product), is energetically less favored due to potential clashes with the active site cleft residues, including helix α5. The Y229A mutant protein showed only a marginal reduction in the efficiency of hydrolysis of bis-*p*NPP, but 2′,3′-cAMP and 3′,5′-cAMP were both poorly hydrolyzed (Fig. 4*E*). Thus, despite the lack of direct hydrogen bonds between the protein and purine ring/ribose of 3′,5′-cAMP, the Y229A mutation may disrupt a network of water molecules between Tyr^{229} and the phosphodiester bond of 3′,5′-cAMP, as seen in the crystal structure of the 5′-AMP complex (Fig. 3*D*).

His^{209} is another highly conserved residue in MPEs and coordinates Fe^{3+} in Rv0805. This residue is positioned almost opposite to His^{98}, with the metal ion pair between them. Docked positions of 3′,5′-cAMP and bis-*p*NPP places them between His^{98} and His^{209} such that either residue could influence the hydrolysis of these substrates. According to the model 2′,3′-cAMP may be placed farthest (Fig. 4*C*), and with the least favorable orientation toward the His^{209} side chain. In agreement with this, mutation of His^{209} to Ala significantly decreased the hydrolysis of 3′,5′-cAMP and bis-*p*NPP (Fig. 4*E*), but not 2′,3′-cAMP.

Current docking analysis showed that His^{140} was placed at some distance from the substrates (Fig. 4). This positioning is in contrast to what was observed in the Rv0805$^{1-278}$ structure (14) (supplemental Fig. S3) where the different modes of binding of substrates was a result of the absence of the C terminus and, consequently, the structured loops Gly^{26}–Val^{35} and Tyr^{229}–Gln^{247}. We re-investigated the catalytic properties of the H140A mutant protein using protein purified with metal supplementation in the media. No alteration in catalytic activity was seen with any of the substrates and the H140A mutant protein (Fig. 4*E*), in agreement with current docking analysis that indicates a minimal role for His^{140} in substrate interaction. Earlier preparations of the H140A mutant showed a marked loss of activity toward 3′,5′-cAMP (14) and we attribute the current result to the possibility that subtle conformational changes in the active site may occur if the Rv0805 is produced and folded in the presence or absence of metals.

Expression of Rv0805 in Mycobacteria Results in Perturbations of cAMP Levels and Cell Wall Permeability—Although Rv0805 may cleave cAMP *in vivo* and *in vitro*, given its promiscuity in recognizing structurally diverse substrates, it is likely that there are additional components in mycobacterial cells that either serve as substrates for Rv0805 or modulate its activity within the cell. We monitored the expression of Rv0805 in subcellular fractions prepared from *M. tuberculosis* by Western blot analysis, and found that a large fraction was localized to the cell membrane and the cell wall, with a minor amount seen in the cytosol (Fig. 5*A*). Our results are in contrast to those reported recently (4) where FLAG-tagged Rv0805 expressed in *M. tuberculosis* was found to be predominantly intracellular. If one assumes that the major role for Rv0805 in the cell would be

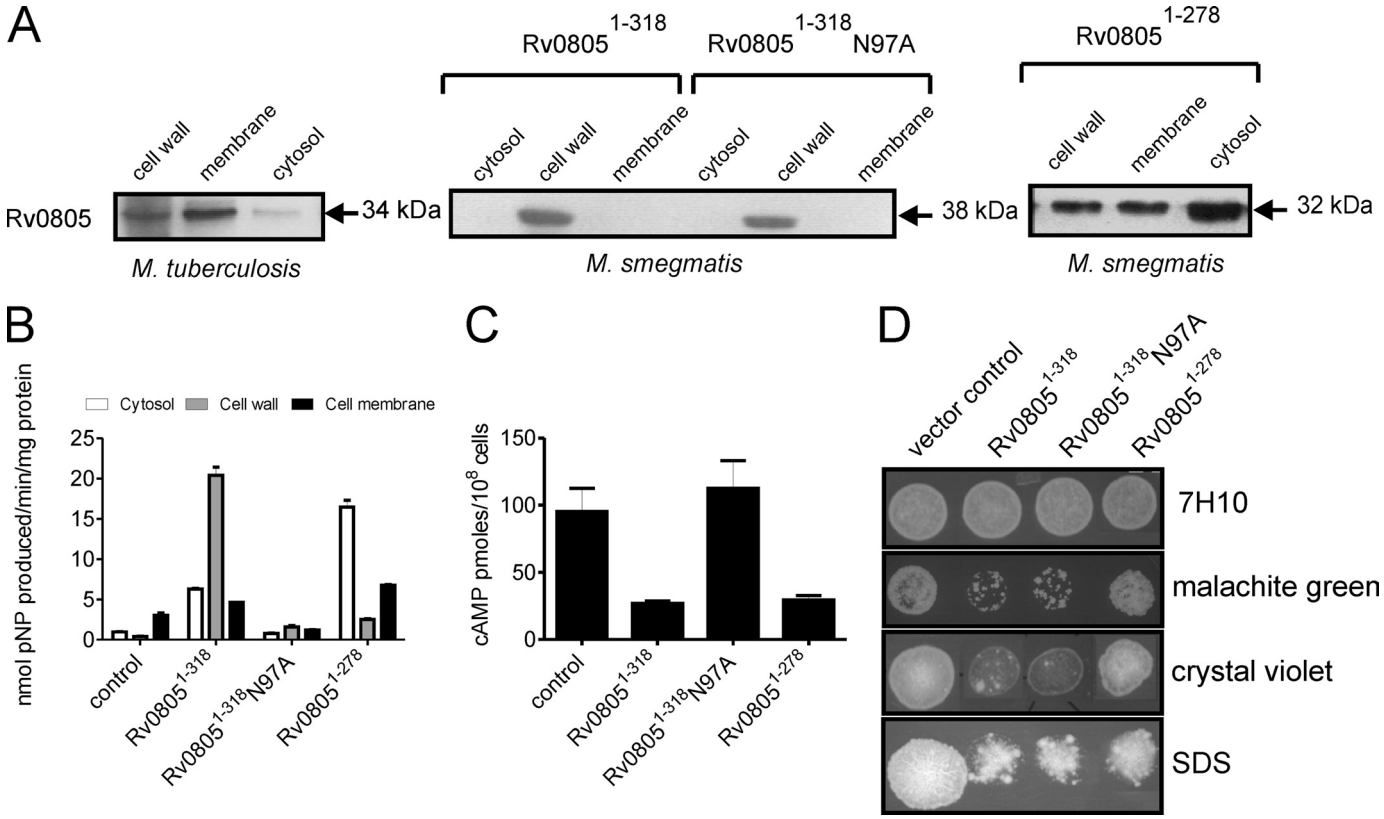

FIGURE 5. **Subcellular localization and function of Rv0805$^{1-318}$ and Rv0805$^{1-278}$ in mycobacteria.** *A*, subcellular fractions (50 μg of protein) of *M. tuberculosis* were subjected to Western blot analysis using a monoclonal antibody to Rv0805. His-tagged wild type or mutant Rv0805$^{1-318}$ or Rv0805$^{1-278}$ were expressed in *M. smegmatis* and subcellular fractions prepared. Protein (50 μg) was subjected to Western blot analysis using a monoclonal antibody to Rv0805. The molecular sizes indicated include the addition of additional residues coming from the His_6 tag and vector. *B*, protein (50 μg) was taken for assay using bis-*p*NPP as a substrate. Note that expression of Rv0805$^{1-278}$ was higher in cells than that of Rv0805$^{1-318}$ (*panel A*), but the activity with bis-*p*NPP is lower for Rv0805$^{1-278}$ than Rv0805$^{1-318}$ (see Table 2). Subcellular fractions prepared from a strain of *M. smegmatis* transformed with the control vector (*control*) was used to detect background activity. *C*, intracellular cAMP was measured in a control strain of *M. smegmatis*, and in strains expressing wild type or mutant Rv0805$^{1-318}$ proteins or Rv0805$^{1-278}$. Cells were harvested at late-log phase for cAMP measurements. *D*, cells (10^7) of the indicated strains were spotted on 7H10 agar plates containing 5 μg/ml of malachite green, 10 μg/ml of crystal violet, or 0.01% SDS and incubated for 2–3 days, after which the plates were photographed.

to hydrolyze intracellular cAMP, localization in the cell wall is intriguing.

We used the knowledge obtained from the structure and activities of Rv0805$^{1-318}$ and Rv0805$^{1-278}$, and the information obtained from structure-based mutational analyses, to delineate the roles of Rv0805 in the cell. We expressed Rv0805$^{1-318}$ and Rv0805$^{1-278}$ wild type proteins as well as the catalytically dead N97A mutant full-length protein in *M. smegmatis*, which has no close ortholog of Rv0805 encoded in its genome (6). No difference in growth rate or colony morphology was seen in cells overexpressing Rv0805 (data not shown). Expression of wild type Rv0805$^{1-318}$ or the N97A mutant in *M. smegmatis* resulted in its localization predominantly to the cell wall with very little seen in the membrane and cytosol fractions. Expression of Rv0805$^{1-278}$ was consistently higher than the full-length enzyme in cells (~5-fold based on immunoreactivity), with the majority found in the cytosol, and some in the membrane and cell wall fractions (Fig. 5*A*). Therefore, the C-terminal region of Rv0805 aids in more efficient localization of the protein to the cell wall, perhaps by acting as a recognition motif for components of the secretory machinery. Moreover, the fact that the last 20 amino acids are unstructured could suggest that this stretch of amino acids contains an interaction motif assisting in localization of the protein.

Rv0805 expressed in *M. smegmatis* was catalytically active, because increased hydrolysis of bis-*p*NPP was seen in subcellular fractions over and above that seen in control cells (Fig. 5*B*). Increased phosphodiesterase activity seen in the cytosolic fractions of cells expressing Rv0805$^{1-278}$ was commensurate with its high level of expression in this cellular compartment. No significant hydrolysis of bis-*p*NPP over and above that seen in vector-transformed cells was seen in fractions prepared from cells expressing the N97A mutant protein, as would be expected from its low catalytic activity (Fig. 4*E*). We also monitored cAMP levels in cells expressing either Rv0805$^{1-318}$ or Rv0805$^{1-278}$ (Fig. 5*C*). A reduction in intracellular cAMP was seen in both cells to equivalent extents. As expected, expression of the catalytically inactive N97A mutant protein did not lead to a decrease in intracellular cAMP levels.

The specific and unusual localization of Rv0805 in the cell wall could suggest that hydrolysis of substrates for Rv0805 in that subcellular compartment may perturb and alter cell wall permeability. We tested the sensitivity of *M. smegmatis* strains overexpressing Rv0805$^{1-318}$ or Rv0805$^{1-278}$ to malachite green and crystal violet, two lipophilic inhibitors of cell growth that have been used to screen for cell wall perturbations in mycobacteria (28, 29) and SDS. As seen in Fig. 5*D*, cells expressing Rv0805$^{1-318}$ were highly sensitive to malachite green, crystal violet, and SDS.

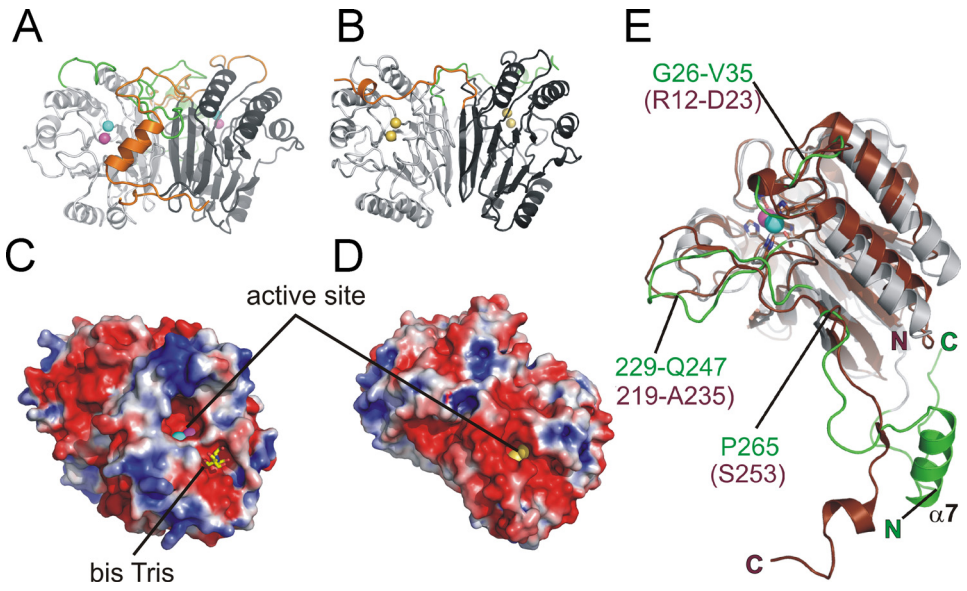

FIGURE 6. **Comparison of the Rv0805$^{1-318}$-fold with GpdQ.** *A*, Rv0805$^{1-318}$ dimer as a ribbon representation (colored as described in the legend to Fig. 1). *B*, GpdQ (3D03) dimer, ribbon representation. The MPE domains are in *light* and *dark gray*, as in Rv0805. The GpdQ cap domain Ser^{253}–Arg^{274} is colored *orange* or *green*. Cobalt ions in the GpdQ active site are in *yellow*. *C*, electrostatic surface of Rv0805$^{1-318}$; and *D*, electrostatic surface of GpdQ dimer (PDB 3D03). Calculations were done using the Poisson-Boltzmann equation (APBS) (33). Cut off −2.5 kT/e was used for negative potential (*red*) and 2.5 kT/e for positive potential (*blue*). Active site metals are shown as *spheres*. Rv0805 and GpdQ are symmetric homodimers related by 180° axis, therefore in the present view, only one active site of the two can be seen. Bis-Tris bound to Rv0805$^{1-318}$ is shown in *sticks* (carbon, *yellow*; oxygen, *red*; nitrogen, *blue*). *E*, superposition of Rv0805$^{1-318}$ (*gray green*) and GpdQ (3d03; chain A) (*brown*) monomers. Active site metal ions of the two structures superimpose very closely, therefore for clarity, only Fe^{3+} (*cyan*) and Mn^{2+} (*magenta*) of Rv0805$^{1-318}$ are shown as *spheres*. Residues in Rv0805 are marked in *green*, and in *brown* for GpdQ. The structural alignment in *E* was done according to Ref. 31.

Most unexpectedly, sensitivity was still seen in cells expressing the N97A mutant protein, indicating that the increased sensitivity was brought about by Rv0805 in a catalytically independent manner. Moreover, cells expressing Rv0805$^{1-278}$ were as resistant as control cells to malachite green and crystal violet, and showed some resistance to SDS. It is to be noted that the absolute amount of Rv0805$^{1-278}$ in the cell wall fraction was similar to Rv0805$^{1-318}$ as monitored by Western blotting (Fig. 5*A*). Therefore, the perturbations induced in the cell wall on expression of Rv0805$^{1-318}$ may not solely be a result of its presence in the cell wall, but also critically dependent on the residues beyond Pro^{278}. Thus, the C terminus of Rv0805 is important not only for modeling the active site to accommodate more linear substrates/regulatory molecules that may be present in the cell, but also to modulate cell wall properties in a manner independent of the catalytic activity of the enzyme.

In conclusion, whereas cAMP production by mycobacteria has been shown to be important for the virulence of *M. tuberculosis* (4), we suggest that an additional role of Rv0805 in mycobacteria is independent of its ability to hydrolyze cAMP. Because the gene encoding Rv0805-like protein is found only in pathogenic mycobacteria, and is predicted to be a functional protein in *M. leprae* (which has undergone a large degree of pseudogenization), Rv0805 may play a critical role in the pathogenicity of mycobacteria, not only by hydrolyzing cAMP in the cell, but also "moonlighting" as a cell wall remodeling protein.

DISCUSSION

In the current study we report structures of the Rv0805 protein alone and in complex with 5′-AMP, revealing unique features that could account for its promiscuous substrate selection and putative role in modeling the cell wall. Because Rv0805 does not seem to possess a classical signal sequence, its localization to the cell membrane and cell wall could be via a specialized secretion system operative in mycobacteria. It appears that the C-terminal domain of Rv0805 is used to better adjust the substrates into the active site as well as facilitate subcellular localization of the protein. Because the last 20 residues of Rv0805$^{1-318}$ remain disordered in the crystal, we propose that the floppy nature of this peptide may serve as an anchor for Rv0805 to interact with either the mycobacterial membrane or cell wall, or to other proteins. Further studies directed toward this aspect are ongoing in the laboratory.

The structure of Rv0805 is strikingly similar to another MPE family member, glycerophosphodiesterase (GpdQ) (11, 30) from *Enterobacter aerogenes*, which cleaves mono-, di- and triphosphoesters, with glycerophosphoethanolamine proposed to be its natural substrate. Using the Protein Structure Comparison Service (SSM) at the European Bioinformatics Institute (31), the r.m.s. deviation values were calculated for the core regions of both structures, using the CA atoms of residues Val^{15}–Pro^{265} of Rv0805, and Leu^{2}–Ser^{253} of GpdQ (PDB 3D03). The r.m.s. deviation value between the monomer structures of Rv0805 and GpdQ (chain A) was 1.8 Å and between the dimers (using chains A and B of 3D03) was 2.1 Å. Especially impressive is the similarity of the homodimer interface in both proteins (Fig. 6), seen so far in only these two proteins. The highly conserved residues of the MPE active site are well superposed between the two proteins (Fig. 6*E*), but major structural differences in Rv0805$^{1-318}$ and GpdQ are in the region of loops Tyr^{229}–Gln^{247} and Val^{219}–Ala^{235}, respectively, the C termini beyond residue Pro^{265} in Rv0805 and Ser^{253} in GpdQ, as well as at the extreme N terminus, which is significantly shorter in the GpdQ structure (Fig. 6*E*). GpdQ forms a trimer of dimers that may further help regulate its substrate specificity. Both Rv0805 and GpdQ have negatively charged active sites but the overall distribution of the electrostatic charge in Rv0805$^{1-318}$ is significantly different to GpdQ (Fig. 6, *C* and *D*). Adjacent to the active site, Rv0805$^{1-318}$ contains another negatively charged cleft, observed as the bis-Tris binding region (Fig. 6*C*), encircled by a rim of positively charged residues that build a plateau-shaped solvent-exposed

surface, which may have significance in interaction with cell wall components of mycobacteria.

Crystal structures of $Rv0805^{1-318}$ alone and in complex with 5′-AMP, together with molecular docking and accompanying biochemical analysis, now provide a possible explanation for the observed substrate promiscuity of the Rv0805. The Rv0805 active site is broad enough to accept small molecules with a cyclic or linear phosphodiester bond, but which side of the phosphodiester bond is cleaved depends on the geometry of the substrate and its binding orientation (see Table 2 and Fig. 4). Interestingly, *in vitro*, linear phosphodiesters seemed to be kinetically more favored by $Rv0805^{1-318}$ than cyclic substrates. Docking experiments show that bis-*p*NPP is anchored to the active site only via its phosphate moiety, with no significant interactions with the rest of the protein. It seems likely that the shape of the $Rv0805^{1-318}$ active site, rather than specific residues, allow linear substrates to bind with an orientation that enables more effective hydrolysis than the cyclic phosphodiester substrates. The mechanism of hydrolysis of cyclic phosphodiesters may follow that proposed for Mre11 (7, 32), with His^{98} as a crucial residue coordinating the transition state complex. On the other hand, His^{209} may take this role in the case of linear substrates (Fig. 4).

The role of Rv0805 in the biology of pathogenic bacteria is not known. A recent report has utilized the overexpression of Rv0805 in *M. tuberculosis* as a means of regulating cAMP levels in the bacterial cell and thereby transcription of tumor necrosis factor α (4). In these studies, N-terminal FLAG-tagged Rv0805 was predominantly localized to the cytosol with some seen in the particulate fraction of cells. This is in contrast to our results, where Rv0805 in *M. tuberculosis* and *M. smegmatis* was preferentially localized to the cell envelope. Because we now show that Rv0805 can alter the properties of the cell wall, the low virulence seen of *M. tuberculosis* overexpressing Rv0805 in earlier studies (4) could also perhaps be attributed to modifications in the cell wall of the bacteria, in addition to lowering intracellular cAMP levels.

There is additional, albeit circumstantial evidence, for a role of Rv0805 in regulating cell wall processes in *M. tuberculosis*. In a recent study to identify new analogs of trichlosan that could act as inhibitors of the enol reductase InhA (33), genes were identified that were up-regulated in the presence of these inhibitors. Most of these genes were those involved in fatty acid and cell wall biosynthesis and Rv0805 was also up-regulated 1.5-fold. With the background of the data presented here, the association of Rv0805 with a gene regulatory network associated with cell wall function may not be coincidental.

A recent study to identify proteins in *M. tuberculosis* that allowed the bacterium to withstand acidic conditions present in the phagosome identified 21 transposon insertion mutants that were sensitive to medium acidification (34). More than 70% of these mutants were in genes that are annotated as being involved in cell wall functions, such as peptidoglycan and lipoarabinomanan biosynthesis. One transposon mutant contained an insertion within the *rv0805* gene. Once again, there is suggestive evidence that the major role of Rv0805 could be related to cell wall function, in assisting the bacterium to respond to varied stress conditions.

Although the precise role of Rv0805 in mycobacteria is still not known, the structural and biochemical details that we have provided here strongly suggests that whereas one of its substrates in the cell could indeed be cAMP, surface electrostatics and binding sites for other molecules (*i.e.* bis-Tris (Fig. 6*C* and supplemental Fig. S3)), indicate that there could be other substrates for Rv0805. More intriguingly, Rv0805 may alter properties of the cell wall of mycobacteria in a catalytically independent manner, perhaps by acting as a scaffold as seen for Vps29 (13). Because the mycobacterial cell wall is unique in its composition and believed to play an important role in cellular physiology and pathophysiology, further studies on the role of Rv0805 in mycobacteria are warranted. The availability of information in atomic detail on the active site of Rv0805 should allow the development of novel inhibitors of Rv0805. These can be used to dissect the catalytic roles for Rv0805 in the cell, independently of its other non-catalytic functions that result from unique structural elements present in the protein.

Acknowledgments—We acknowledge the help of Maja Capuder and Petra Draškovič at various stages of this study. We thank the staff at the synchrotron facilities at EMBL/DASY, Hamburg, Germany, and XRD beamline, Elettra, Trieste, Italy, for support with the data collection of various forms of Rv0805 crystals. We also thank Dr. Avinash R. Shenoy for critical reading of the manuscript.

REFERENCES

1. Ehrt, S., and Schnappinger, D. (2009) *Cell. Microbiol.* **11,** 1170–1178
2. Shenoy, A. R., and Visweswariah, S. S. (2006) *FEBS Lett.* **580,** 3344–3352
3. Shenoy, A. R., and Visweswariah, S. S. (2006) *Trends Microbiol.* **14,** 543–550
4. Agarwal, N., Lamichhane, G., Gupta, R., Nolan, S., and Bishai, W. R. (2009) *Nature* **460,** 98–102
5. Conti, M., and Beavo, J. (2007) *Annu. Rev. Biochem.* **76,** 481–511
6. Shenoy, A. R., Sreenath, N., Podobnik, M., Kovacevic, M., and Visweswariah, S. S. (2005) *Biochemistry* **44,** 15695–15704
7. Hopfner, K. P., Karcher, A., Craig, L., Woo, T. T., Carney, J. P., and Tainer, J. A. (2001) *Cell* **105,** 473–485
8. Voegtli, W. C., White, D. J., Reiter, N. J., Rusnak, F., and Rosenzweig, A. C. (2000) *Biochemistry* **39,** 15365–15374
9. Keppetipola, N., and Shuman, S. (2008) *J. Biol. Chem.* **283,** 30942–30949
10. Richter, W. (2002) *Proteins* **46,** 278–286
11. Jackson, C. J., Carr, P. D., Liu, J. W., Watt, S. J., Beck, J. L., and Ollis, D. L. (2007) *J. Mol. Biol.* **367,** 1047–1062
12. Hierro, A., Rojas, A. L., Rojas, R., Murthy, N., Effantin, G., Kajava, A. V., Steven, A. C., Bonifacino, J. S., and Hurley, J. H. (2007) *Nature* **449,** 1063–1067
13. Collins, B. M., Skinner, C. F., Watson, P. J., Seaman, M. N., and Owen, D. J. (2005) *Nat. Struct. Mol. Biol.* **12,** 594–602
14. Shenoy, A. R., Capuder, M., Draskovic, P., Lamba, D., Visweswariah, S. S., and Podobnik, M. (2007) *J. Mol. Biol.* **365,** 211–225
15. Tyagi, R., Shenoy, A. R., and Visweswariah, S. S. (2009) *J. Biol. Chem.* **284,** 5217–5228
16. Shenoy, A. R., and Visweswariah, S. S. (2003) *Anal. Biochem.* **319,** 335–336
17. Otwinowski, Z., and Minor, W. (1997) *Methods Enzymol.* **276,** 307–326
18. Collaborative Computational Project, Number 4 (1994) *Acta Crystallogr. D Biol. Crystallogr.* **50,** 760–763
19. Jones, T. A., Zou, J. Y., Cowan, S. W., and Kjeldgaard, M. (1991) *Acta Crystallogr. A* **47,** 110–119
20. DeLano, W. L. (2002) *The PyMOL Molecular Graphics System*, DeLano Scientific LLC, Palo Alto, CA
21. Weininger, D. (1988) *J. Chem. Inf. Comput. Sci.* **28,** 31–36
22. Delogu, G., Bua, A., Pusceddu, C., Parra, M., Fadda, G., Brennan, M. J., and Zanetti, S. (2004) *FEMS Microbiol. Lett.* **239,** 33–39

23. Dass, B. K., Sharma, R., Shenoy, A. R., Mattoo, R., and Visweswariah, S. S. (2008) *J. Bacteriol.* **190,** 3824–3834
24. Rezwan, M., Lanéelle, M. A., Sander, P., and Daffé, M. (2007) *J. Microbiol. Methods* **68,** 32–39
25. Zor, T., and Selinger, Z. (1996) *Anal. Biochem.* **236,** 302–308
26. Shenoy, A. R., Sreenath, N. P., Mahalingam, M., and Visweswariah, S. S. (2005) *Biochem. J.* **387,** 541–551
27. Ding, F., Prutzman, K. C., Campbell, S. L., and Dokholyan, N. V. (2006) *Structure* **14,** 5–14
28. Liu, J., and Nikaido, H. (1999) *Proc. Natl. Acad. Sci. U.S.A.* **96,** 4011–4016
29. Kana, B. D., Gordhan, B. G., Downing, K. J., Sung, N., Vostroktunova, G., Machowski, E. E., Tsenova, L., Young, M., Kaprelyants, A., Kaplan, G., and Mizrahi, V. (2008) *Mol. Microbiol.* **67,** 672–684
30. Hadler, K. S., Tanifum, E. A., Yip, S. H., Mitić, N., Guddat, L. W., Jackson, C. J., Gahan, L. R., Nguyen, K., Carr, P. D., Ollis, D. L., Hengge, A. C., Larrabee, J. A., and Schenk, G. (2008) *J. Am. Chem. Soc.* **130,** 14129–14138
31. Krissinel, E., and Henrick, K. (2004) *Acta Crystallogr. D Biol. Crystallogr.* **60,** 2256–2268
32. Williams, R. S., Moncalian, G., Williams, J. S., Yamada, Y., Limbo, O., Shin, D. S., Groocock, L. M., Cahill, D., Hitomi, C., Guenther, G., Moiani, D., Carney, J. P., Russell, P., and Tainer, J. A. (2008) *Cell* **135,** 97–109
33. Boyne, M. E., Sullivan, T. J., amEnde, C. W., Lu, H., Gruppo, V., Heaslip, D., Amin, A. G., Chatterjee, D., Lenaerts, A., Tonge, P. J., and Slayden, R. A. (2007) *Antimicrob. Agents Chemother.* **51,** 3562–3567
34. Vandal, O. H., Pierini, L. M., Schnappinger, D., Nathan, C. F., and Ehrt, S. (2008) *Nat. Med.* **14,** 849–854